Journal of *Marine Science and Engineering*

MDPI

Article

The Structure and Function of the *Sargassum fusiforme* Microbiome under Different Conditions

Chunchun Dai [1,2] and Shengqin Wang [1,2,*]

[1] College of Life and Environmental Science, Wenzhou University, Wenzhou 325035, China
[2] Zhejiang Provincial Key Laboratory for Water Environment and Marine Biological Resources Protection, Wenzhou University, Wenzhou 325035, China
* Correspondence: mysango@163.com

Abstract: Brown macroalgae, a key component of the vegetated coastal ecosystems, can sequester a large amount of CO_2, which is mainly converted to polysaccharides. These polysaccharides confer complex structures and are difficult to be degraded by microbial communities. On the surface of brown macroalgae in which bacteria lived, the diversity and encoded enzymes of these bacteria involved in carbon cycling remain largely unknown. In this study, we used metagenomic sequencing to survey bacteria communities associated with the *Sargassum fusiforme* under different conditions and investigated the structure and function of these bacteria. A total of 5308 species were discovered in all 15 samples from different conditions. Most of these species belonged to the phylum Proteobacteria. Many *S. fusiforme*-associated bacteria could decompose algal polysaccharides under different conditions. Our method could enhance the ability to understand the microbiome community. To the best of our knowledge, this is the first report regarding metagenomics in *S. fusiforme*. The co-occurrence network provides insights into the relationship of the polysaccharide degradation enzymes (PDEs). These data provide a reference for the cultivation of *S. fusiforme* and the understanding of the marine carbon cycle.

Keywords: *Sargassum fusiforme*; metagenomics; polysaccharide degrading enzymes

Citation: Dai, C.; Wang, S. The Structure and Function of the *Sargassum fusiforme* Microbiome under Different Conditions. *J. Mar. Sci. Eng.* **2022**, *10*, 1401. https://doi.org/10.3390/jmse10101401

Academic Editor: Carmela Caroppo

Received: 31 August 2022
Accepted: 28 September 2022
Published: 30 September 2022

1. Introduction

As crucial primary producers, macroalgae can sequester hundreds of Tg carbon dioxide globally every year [1] and make a great contribution to climate change mitigation and adaptation [2]. Sargassum is a genus of brown macroalgae that is a key component of vegetated coastal ecosystems [3]. Floating mats of Sargassum macroalgae have increased to generate an 8850-km-long belt containing >20 million metric tons of biomass in the Atlantic Ocean in recent years [4]. The recurrent blooms of Sargassum can sequester a large amount of CO_2, most of which are converted to polysaccharides and play a major role in carbon cycling [5]. The polysaccharides accounting for ~40% of the dry weight, mainly constituted by alginate and fucoidan, confer high complex structure, causing difficulty in microbial community degradation [6–8]. Therefore, research on the characteristics and function of the Sargassum-related microbiome, especially the involved polysaccharide degradation enzymes (PDE), is essential for understanding the degradation and recycling of marine carbon.

Bacteria are abundant on the surface of brown macroalgae, with a density of about 1.1×10^8 organisms per cm^2 [9]. These bacteria encode degradative enzymes to transform carbohydrates for nutritional purposes when living in a nutrient-limited state or dead algae, thus contributing to the recycling of marine carbon. In the isolated surface microbiota of brown seaweed *Ascophyllum nodosum*, a quarter can act on at least one type of polysaccharides, most of which are assigned to the Gammaproteobacteria and Flavobacteriia classes based on the 16s rRNA information [10]. Whole genome sequencing was also used to discover polysaccharides degrading bacteria with high alginolytic activity in the rotten

Sargassum fusiforme [11]. However, there is limited information on the microbiome involved in degrading brown-algae polysaccharides.

The structure of brown-algae polysaccharide is different from that present in terrestrial environments. The PDEs involved in marine bacteria should also be different. Many new PDEs have been purified, and activity assays were performed from marine bacteria [12]. Genome mining can also detect candidate PDEs by a curated reference database [13]. The CAZy database is a knowledge-based resource widely used for annotating carbohydrate-active enzymes [14]. According to the sequence similarity of catalytic modules, cellulases are classified into several glycoside hydrolase (GH) families, and alginate lyases are lodged into a dozen of polysaccharide lyases (PL) families (www.cazy.org, accessed on 15 August 2022). Some families of the alginate lyases have been mostly isolated from marine organisms, such as PL7, PL15, and PL17 [15].

S. fusiforme, known as brown macroalgae, grows in the lower intertidal zones along the Pacific Northwest coastlines [16]. The alginate comprised in *S. fusiforme* (~30% of dry weight) is larger than that in kelp (~25%) [17,18]. However, the taxonomy and function of the related microbiome are poorly known. The exploration of metagenomic sequencing of marine environments provides the promise of massive screening of microbiome community structure and candidate PDE enzymes [19,20]. In this study, we evaluated the individual and combined effects of salinity and oxygen on the *S. fusiforme*-related microbiota. We demonstrated microbial diversity, community structure and function, and PDE co-occurrence network under different conditions using metagenomic technology, providing a reference for the cultivation of *S. fusiforme* and the understanding of the marine carbon cycle.

2. Materials and Methods

2.1. Sample Collection and Whole Metagenome Sequencing

Samples for metagenomic sequencing were obtained from rotten vesicles of *S. fusiforme* cultivated in the Wenzhou Dongtou District, Zhejiang Province of China (27.82° N, 121.18° E) (Table 1). The isolates were randomly collected at the southeast-facing shallow sea on 28 May 2020. Three isolates were cultivated in seawater (salinity of 30‰) for two days. For each of them, we divided it into five parts. One part was stored in the −80 °C ultra-low temperature freezers, and the other four parts were cultivated in four different conditions for 10 additional days: Seawater + Air; Seawater; Freshwater + Air; and Freshwater (Table 1). These 12 samples were frozen at −80 °C. The total microbial genomic DNA of these samples was extracted by the Magnetic Soil and Stool DNA Kit (Tiangen Biotech Co., Ltd., Beijing, China), and the quantity and integrity were confirmed by NanoDrop, Qubit 2.0, and 1% agarose gel electrophoresis. Metagenomic sequencing was conducted with a 150 bp paired-end on the Illumina HiSeq platform (Novogene Bioinformatics Technology Co., Ltd., Beijing, China).

Table 1. Sample information.

Samples	/	Seawater (2 d)			
		Seawater + Air (10 d)	Seawater (10 d)	Freshwater + Air (10 d)	Freshwater (10 d)
Isolate 1	A1	B1	C1	D1	E1
Isolate 2	A2	B2	C2	D2	E2
Isolate 3	A3	B3	C3	D3	E3

2.2. Sequencing Data Processing, Assembly and Gene Annotation

Quality control was performed by the KneadData tool (version 0.10.0) (https://huttenhower.sph.harvard.edu/kneaddata/, accessed on 23 June 2022), which integrates the tool Trimmomatic (version 0.33) [21] and Bowtie 2 [22] for quality filtering and host DNA decontamination. The clean data was assembled with MEGAHIT (V1.2.9) to acquire contigs with default parameters [23]. The clean data were realigned to the assembled contigs to get

the unmapped reads by Bowite 2 [22]. QUAST was implemented to evaluate assembly quality [24]. To minimize the effect of low abundance, we implemented an additional mixed assembly by combining all unmapped reads from each sample with MEGAHIT.

All obtained contigs were subjected to prodigal (V2.6.3,-p meta -m) for the prokaryotic gene prediction [25]. The predicted genes >100 nt were subjected to CDHIT (V4.8.1, -c 0.95 -n 10 -aS 0.9 -aL 0.9 -d 0 -M 0) to remove redundancy and get the initial gene catalog [26], which was used to build reference gene database for following analysis by bowtie2-build (V2.4.5) [22]. The clean data from each sample were aligned to this reference gene database with parameters: -I 200-X 400. A unigene was considered present when at least 10 mapped reads were detected in each of the 6 samples.

We calculated the relative abundance of a unigene k in a sample by a modified formula from a previous study [27]:

$$G_k = \frac{x_k}{L_k} \times \frac{1}{\sum_{i=1}^{n} \frac{x_i}{L_i}} \times 10^6, \quad (1)$$

G_k: The relative abundance of unigene k.
L_k: The lenth of unigene k.
x_k: The number of mapped reads by unigene k.
n: The total number of unigenes.

2.3. Taxonomic Assignment and Diversity

The unigene dataset was aligned to the National Center for Biotechnology Information (NCBI) Non-redundant (NR) protein database by using DIAMOND (V2.0.14) with an e-value of 1e-5 [28]. The aligned output was subjected to MEGAN (V6.21.7) to determine the taxonomic level of each gene by the lowest common ancestor (LCA) algorithm [29]. The relative abundance of each taxonomic level was calculated using the Pandas library with concat function in Python. The Shannon diversity index was calculated by QIIME 2 to measure the diversity of species in a community [30]. Linear discriminant analysis effect size (Lefse) analysis was used to find the different genes and species among groups [31].

2.4. Gene Functional Classification and Polysaccharide Degrading Enzymes Detecting

EggNOG-mapper was used to predict gene functional classification by querying unigenes against annotation sources, including Gene Ontology (GO) labels and Kyoto Encyclopedia of Genes and Genomes (KEGG) pathways [32]. GO enrichment analysis was performed by TopGO with Benjamini-Hochberg correction [33]. The projection of unigenes on the KEGG pathways was done using iPath [34].

To detect candidate PDE genes distributed in *Sargassum*-associated bacteria, we implemented a method previously used to combine sequence alignment and domain search [13]. Reference PDE-related protein sequences were collected from the CAZyme database and literature mining [14]. The catalytic domain information and our unigenes were then located by aligning reference sequences to dbCAN HMMdb v8 by HMMER (V3.3.2, hmmscan-domtblout) [35]. Basic Local Alignment Search Tool (BLAST) was used to find the overlap information between unigenes and the reference sequences with an e-value of 0.001, where at least one matched region with an identity larger than 30% was needed. The PDE gene in unigenes was determined if it matched the following criterion: (1) The same best catalytic domain should be aligned ($\geq$80% of full domain region) for the gene and reference sequence by BLAST search; (2) The relative abundance should be greater than 1 in more than 3 samples.

To analyze the relationship among the PDE genes, metagenomic reads were remapped to detect PDE genes by Bowtie 2 again. To reduce the effect of cross-mapping by a similar sequence, we kept reads with only one best hit for calculating the abundance in PDE genes. The co-occurrence network was visualized in Cytoscape v3.9.1 [36].

3. Results

3.1. Metagenomic Data Assembly and Gene Prediction

Metagenomic sequencing of 15 samples collected from vesicles of *S. fusiforme* resulted in ~984 million clean reads, with an average of ~66 million reads per sample (Supplementary Table S1). About 150 million reads were mapped to the *S. fusiforme* genome and removed. MEGAHIT reconstructed an average of ~123 thousand contigs per sample. The cumulative contig length of each sample was plotted (Figure 1A). Contigs in each sample were split into nonoverlapping 100 bp windows, and the GC content of each window was counted (Figure 1B). The GC content distribution from conditions A and C presented normal distribution, while others presented bimodal distribution, which means that the microbiota structure has dramatically changed in these three conditions.

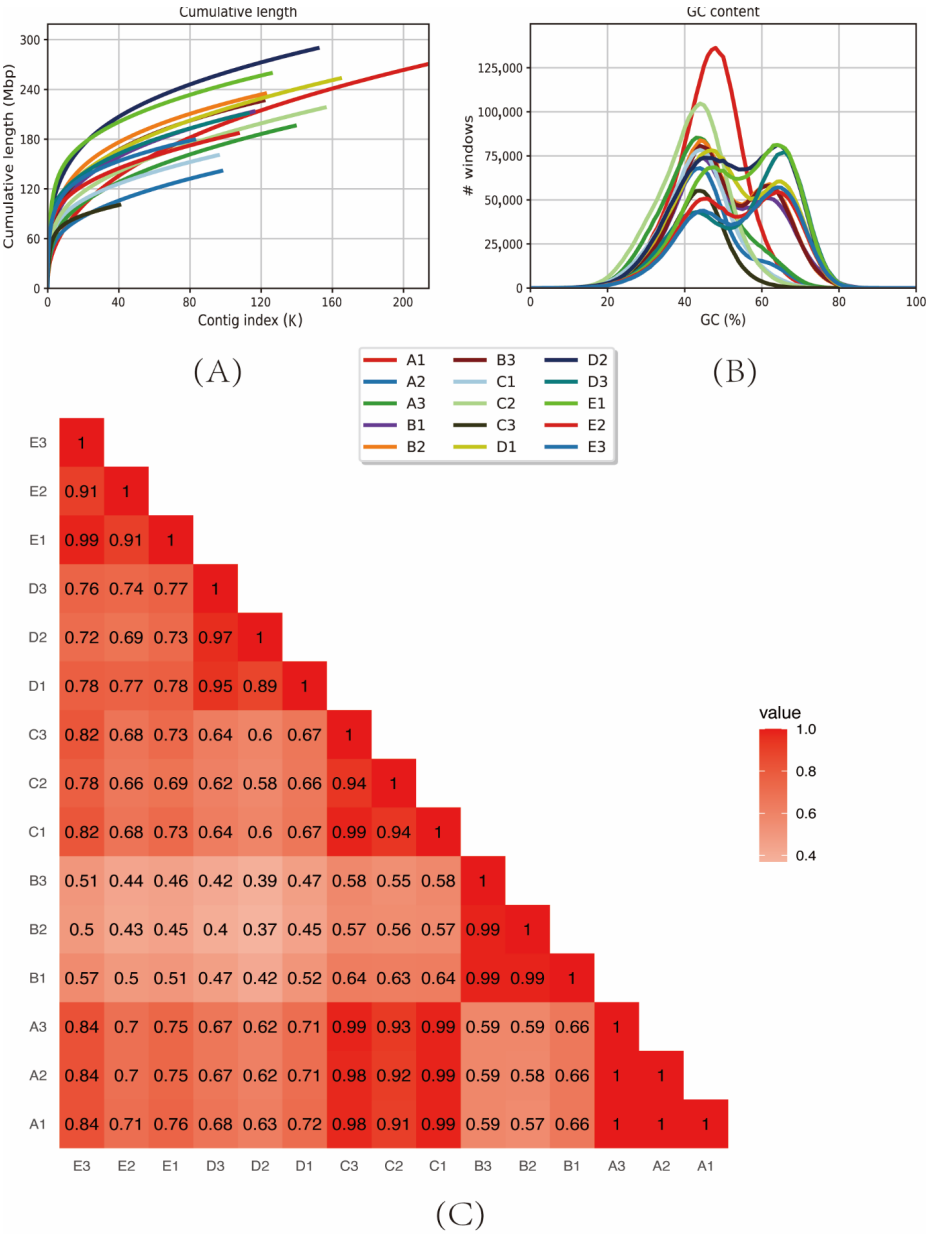

Figure 1. Statistics for the assembly and unigenes. (**A**) The cumulative plot. (**B**) GC content plot. On the *x*-axis, contigs are ordered from the longest to the shortest. The *y*-axis shows the cumulative length. (**C**) Sample correlation plot based on the relative abundance of unigenes. Colors show the Pearson correlation coefficient.

The open reading frames (ORFs) predicted from the prodigal were sent to CD-HIT to get the original gene catalog. After mapping reads by Bowtie, we got 173,411 unigenes after filtering reads in less than 6 samples. The relative abundance of unigenes was calculated in each sample. Gene abundance correlation among the sample was calculated based on the relative abundance of unigenes (Figure 1C). The samples from the same condition had a high correlation coefficient ($\geq$0.89). However, they were different isolates, especially the correlation coefficient from the three samples that were initially collected, which was equal to one, suggesting that the environment had more influence on the *S. fusiforme*-associated microbiome than host genetic information. Samples from conditions A and C had a high correlation coefficient, while a sample from freshwater and seawater had a low correlation coefficient.

3.2. Microbial Community Analysis

Based on the unigenes and LCA algorithm, we detected 5308 species, most of which belong to phylum Proteobacteria, followed by Uroviricota (Supplementary Table S1). About half species were shared by all 15 samples from different conditions, while many species could not be detected by one specific condition (Figure 2A).

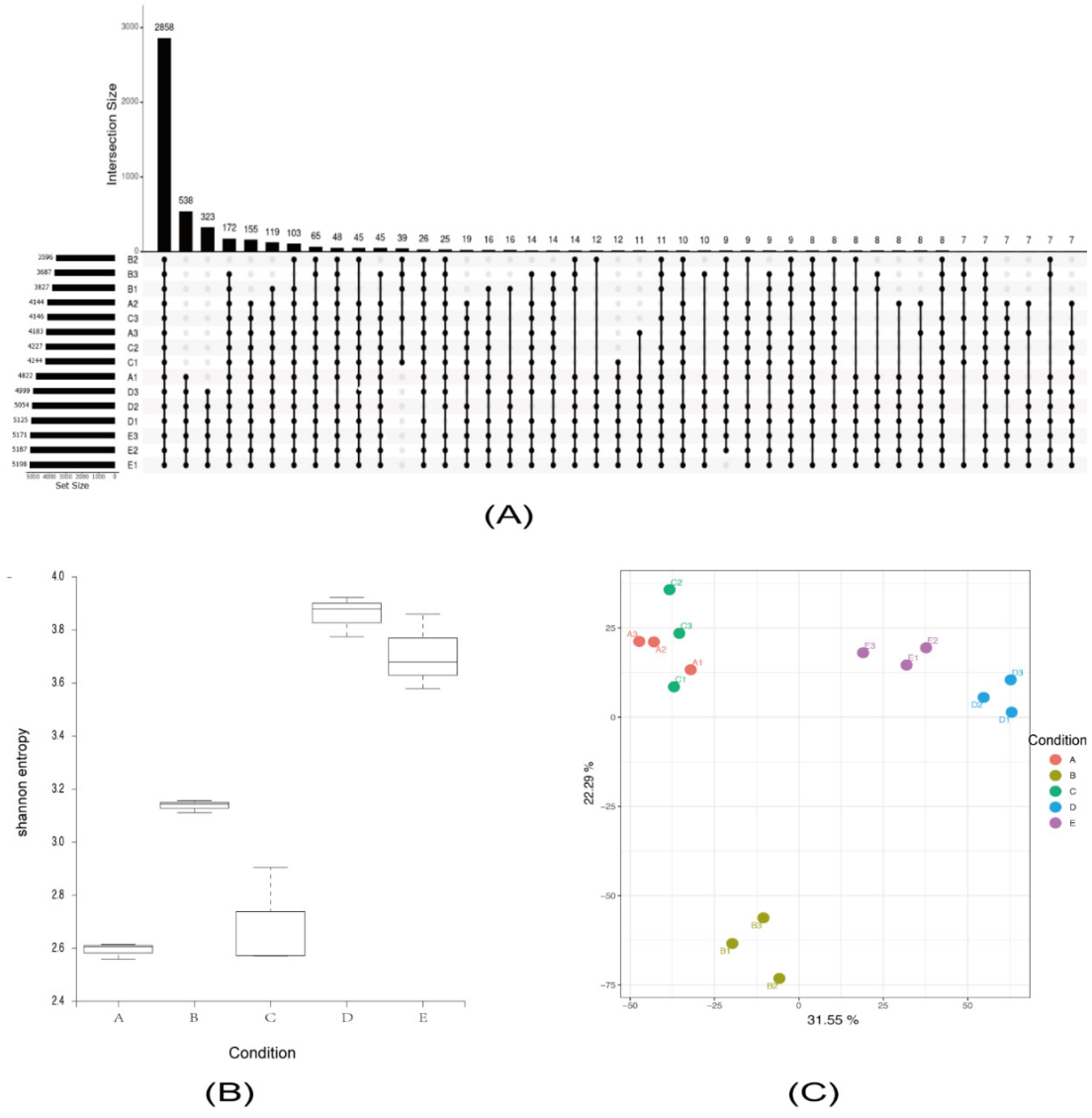

Figure 2. The microbial community analysis of 15 samples. (**A**) Upset plot shows the overlap information of species in each sample; (**B**) Shannon diversity; (**C**) principal component analysis (PCA) plot.

High bacterial diversity was observed among different conditions. Based on the Shannon diversity, the microbiome structure was more complex when the condition changed, and the effect of freshwater should be larger than oxygen (Figure 2B). The microbial community was largely consistent across samples from the same condition, although they belong to different isolates. Conditions A and C were clustered together (Figure 2C). Compared with the samples with air (B and D), the samples from freshwater (D and E) were clustered, suggesting that salinity had a greater effect on *Sargassum*-associated bacteria.

The composition of the *S. fusiforme* microbiome was distinctive across all five conditions, although they shared the same most abundant genus Vibrio (48.5% ± 0.04) (Figure 3A). In all five conditions, A and C had a higher proportion of genus Vibrio; B was enriched with genera Alteromonas and Marinomonas; C had an increased composition of the genus Reinekea; D was enriched with genera Bradyrhizobium, Novosphingobium, and Sphingobium; and E had a higher proportion of genus Sphingomonas (Figure 3B).

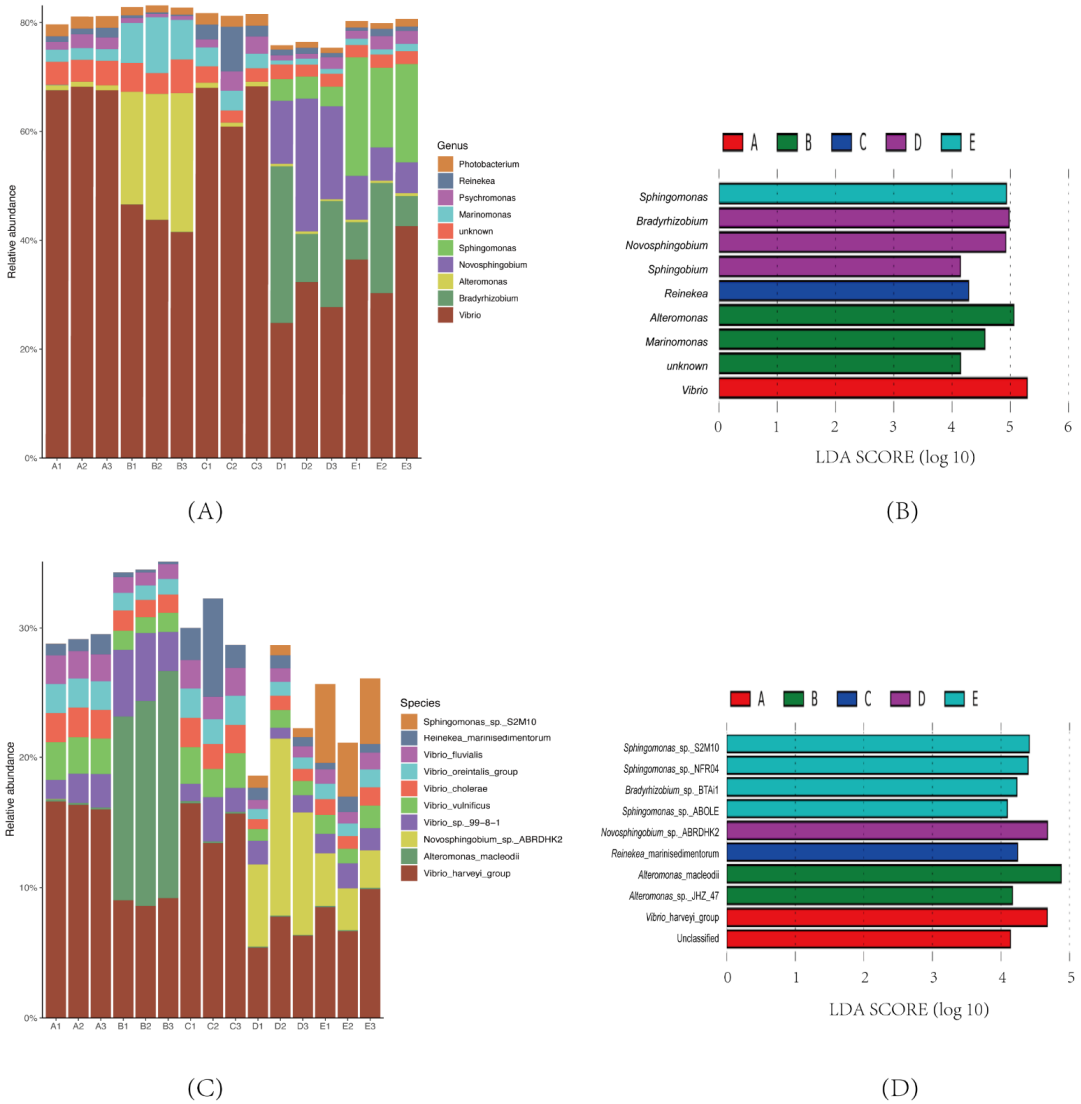

Figure 3. Taxonomic differences in S. fusiforme-related microbiome. Relative abundance bar plots of the top 10 genera (**A**) and linear discriminant analysis (LDA) score plot (score > 4) for microbes among five conditions at genus level (**B**). Relative abundance bar plots of top 10 species (**C**) and LDA score plot (score > 2) for microbes among five conditions at species level (**D**). Linear discriminant analysis effect size (Lefse) analysis was used to find the difference among groups. The LDA value shows the degree.

For species, the *Vibrio harveyi* group (11.1% ± 0.01) was the most abundant species in all treatments, although *Alteromonas macleodii* had a higher abundance in condition B and the *Novosphingobium* sp. ABRDHK2 had a higher abundance in condition D (Figure 3C). For Lefse analysis, the *V. harveyi* group had a higher relative abundance in condition A. *A. macleodii* and *Marinomonas* sp. JHZ_47 were also over-represented in condition B. The *Reinekea marinisedimentorum* and *Novosphingobium* sp. ABRDHK2 were enriched in conditions C and D, respectively. Three *Sphingomonas* and one *Bradyrhizobium* species were enriched in condition E (Figure 3D).

3.3. Gene Function and Polysaccharide Degrading Enzymes Analysis

Differential abundance analysis with Lefse analysis revealed 395 unigenes with significantly different relative abundances among these five conditions, of which 302 and 52 unigenes were enriched in conditions B and D, respectively. GO enrichment analysis of these unigenes showed that the enriched items were related to component/complex assembly (Supplementary Table S2). These unigenes could be matched with 244 KEGG Orthology (KOs), of which 204 and 22 were enriched in conditions B and D, respectively. KEGG pathway suggested that both highly abundant unigenes from conditions B and D enriched in oxidative phosphorylation pathway (Supplementary Figures S1 and S2).

By combing the local alignment and domain search, we detected 205 PDE genes by the top-matched reference sequence, of which 158 and 47 genes were assigned to PL and GH families, respectively. The relative abundance was calculated by the unique mapped reads. Most CAZy families were found in similar proportions in the same group. Most PL genes belong to the PL7 and PL17 families (Figure 4A), and they are highly correlated. A co-occurrence network of the PDE was built by unique mapped reads to search for potential associations (Figure 4B). For $r \geq 0.5$, the final network comprised 128 nodes and 3216 edges, of which 3061 were positive. The PDE genes in the GH107 family had no negative correlation with others. Except for the extremely low abundance family (GH19 and PL5), most of the negative correlations came from the GH18 family, which had 52 negative correlations and 106 positive correlations. For $r \geq 0.8$, the number of edges decreased to 1190, and all correlations were positive (Supplementary Figure S3).

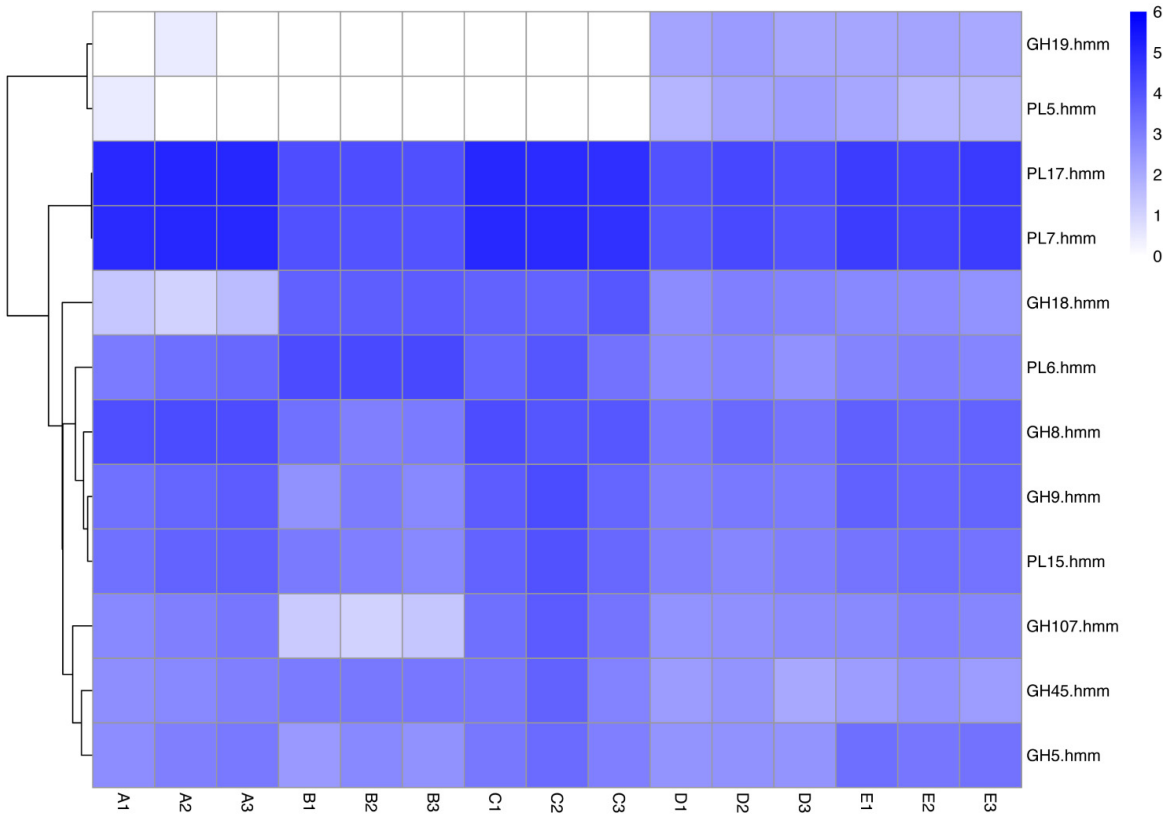

(A)

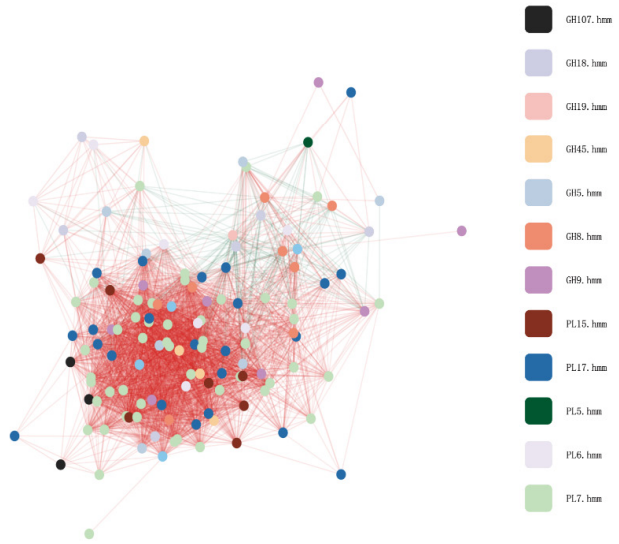

(B)

Figure 4. Relative abundance analysis of polysaccharide degradation enzyme (PDE) family. (**A**) Heatmap showing the relative abundances of the PDE family on a log10 scale. (**B**) Co-occurrence network of the PDE ($r \geq 0.5$). Positive and negative associations are depicted by light red and light green lines, respectively.

4. Discussion

To detect the structure and function of the *S. fusiforme*-associated microbiome, we designed the method using metagenomic sequencing for 15 samples under five conditions. Many species with relatively low abundance in a specific condition are difficult to be detected by metagenomics. Different conditions can enhance the ability to understand the microbiome community (Figure 2A). Metagenomic sequencing from rotten vesicles of *S. fusiforme* contained ~15% host DNA, which suggests that the mixture of tissue and bacterial genomes is an effective way to get bacterial sequences, which are also used in kelp-associated microbiome analysis [37]. The analysis of GC content and microbial community has shown that compared with the change in the environment, the effect of genetic information is still limited. Our previous study also showed low genetic diversity within and between *S. fusiforme populations* [38]. The structure of the *S. fusiforme* microbiome did not change much in the seawater environmental state after 10 days, which supports the difficulty of degradation in the natural state. In this study, 10 days may not be enough to establish a stable structure community for different environmental conditions. However, changes in the environment can dramatically increase the complexity of the microbiome community, and the Shannon diversity and principal component analysis (PCA) plot support that the salinity may have more contribution than oxygen to the variation of Sargassum-associated bacteria (Figure 2B,C). Most differential abundant unigenes were found in conditions B and D, especially for condition B. The air should increase the abundance of aerobic bacteria and the gene enriched in the oxidative phosphorylation pathway (Supplementary Figures S1 and S2). Less differential abundant unigenes were found in the change of salinity through a greater change of microbiome community structure (Figure 2B), which means that the effect of salinity should be broad rather than a few specific species.

Our analysis revealed conditional differences in the relative abundance of certain microbial taxa and PDE families (Figures 3 and 4A). Most Sargassum-associated bacteria belong to the phylum Proteobacteria, which is the dominant organism on brown algal tissue [39]. Some genera were reported to decompose algal polysaccharides, such as Vibrio [40], Alteromonas [41], and Sphingomonas [42]. Vibrio is widespread in marine water, and most of them (>70%) can encode alginate lyases [13]. The isolation of *Vibrio* spp. can cause rot of algae [43], suggesting that the inhibition of this main genus in Sargassum-associated bacteria may reduce the release of ocean carbon. Alteromonas, an important kelp-associated genus, can be disrupted by elevated pCO_2 [44]. *A. macleodii*, which was increased in air condition (Figure 3C), can grow as the largest species in an alginate-supplemented microcosm [45]. *S. fusiforme* grows in intertidal zones, where the salinity regime may change by the effects of the river runoff. Sphingomonas, which was hardly detected in seawater conditions, dramatically increased in freshwater conditions (Figure 3A). Therefore, some *S. fusiforme*-associated bacteria could not be detected by one specific condition, and our method can expand the ability to understand the microbiome community. Bacteria transfer brown algae polysaccharides into inorganic carbon by utilizing a series of diverse PDEs, sometimes hundreds of enzymes [8]. During PDE degradation by marine bacteria, various enzymes are involved in extra- and intercellular degradation pathways. Although the microbiome community changes under different conditions, the high abundance of PDEs was similar (Figure 4A). Both PL7 and PL17 family are broadly available in nature and has endolytic and exolytic alginate lyase activities [15,46]. In the present study, we only detected a few PL15 families, which is thought to be another widely distributed PDE in marine organisms [15]. The network suggests that these PDEs act together (Figure 4B), supporting a pathway for polysaccharide degradation that should require many PDEs [8].

In conclusion, we investigated the individual and combined effects of salinity and oxygen on the *S. fusiforme*-related microbiota, although this study focused only on the early degradation phase, which may change as time increases. The structural analysis of the microbiome detected may condition specific polysaccharide degradation-related bacteria. The genes and PDEs were predicted from the assembled metagenomic data. The co-occurrence network analysis support that encoded PDEs should act together. These data

provide a reference for the cultivation of *S. fusiforme* and the understanding of the marine carbon cycle.

Supplementary Materials: The following supporting information can be downloaded at: https://www.mdpi.com/article/10.3390/jmse10101401/s1, Figure S1: Projection of unigenes enriched in condition B on the KEGG pathways using iPath; Figure S2: Projection of unigenes enriched in condition D on the KEGG pathways using iPath; Figure S3: Co-occurrence network of the PDE ($r \geq 0.8$). Table S1: The species information of *S. fusiforme*-associated microbiome; Table S2: GO enrichment analysis of unigenes with different relative abundances among five conditions.

Author Contributions: Conceptualization, S.W.; methodology, S.W.; formal analysis, C.D.; data curation, C.D.; writing, C.D. and S.W.; supervision, S.W. All authors have read and agreed to the published version of the manuscript.

Funding: This research was supported by the Special Project on Blue Granary Science and Technology Innovation under the National Key R&D Program (2018YFD0901501), the Special Science and Technology Innovation Project for Seeds and Seedlings of Wenzhou City (N20160016), and the Science and Technology Planning Project of Wenzhou City (Y20190210).

Institutional Review Board Statement: Not applicable.

Informed Consent Statement: Not applicable.

Data Availability Statement: Publicly available datasets were analyzed in this study. This data can be found here: https://ngdc.cncb.ac.cn/search/?dbId=gsa&q=PRJCA010165, accessed on 31 August 2022.

Conflicts of Interest: The authors declare no conflict of interest.

References

1. Krause-Jensen, D.; Duarte, C.M. Substantial Role of Macroalgae in Marine Carbon Sequestration. *Nat. Geosci.* **2016**, *9*, 737–742. [CrossRef]
2. Duarte, C.M.; Losada, I.J.; Hendriks, I.E.; Mazarrasa, I.; Marbà, N. The Role of Coastal Plant Communities for Climate Change Mitigation and Adaptation. *Nat. Clim. Chang.* **2013**, *3*, 961–968. [CrossRef]
3. Duarte, C.M.; Gattuso, J.-P.; Hancke, K.; Gundersen, H.; Filbee-Dexter, K.; Pedersen, M.F.; Middelburg, J.J.; Burrows, M.T.; Krumhansl, K.A.; Wernberg, T.; et al. Global Estimates of the Extent and Production of Macroalgal Forests. *Glob. Ecol. Biogeogr.* **2022**, *31*, 1422–1439. [CrossRef]
4. Wang, M.; Hu, C.; Barnes, B.B.; Mitchum, G.; Lapointe, B.; Montoya, J.P. The Great Atlantic Sargassum Belt. *Science* **2019**, *365*, 83–87. [CrossRef] [PubMed]
5. Trevathan-Tackett, S.M.; Kelleway, J.; Macreadie, P.I.; Beardall, J.; Ralph, P.; Bellgrove, A. Comparison of Marine Macrophytes for Their Contributions to Blue Carbon Sequestration. *Ecology* **2015**, *96*, 3043–3057. [CrossRef]
6. Deniaud-Bouët, E.; Kervarec, N.; Michel, G.; Tonon, T.; Kloareg, B.; Hervé, C. Chemical and Enzymatic Fractionation of Cell Walls from Fucales: Insights into the Structure of the Extracellular Matrix of Brown Algae. *Ann. Bot.* **2014**, *114*, 1203–1216. [CrossRef]
7. Arnosti, C. Microbial Extracellular Enzymes and the Marine Carbon Cycle. *Annu. Rev. Mar. Sci.* **2011**, *3*, 401–425. [CrossRef]
8. Sichert, A.; Corzett, C.H.; Schechter, M.S.; Unfried, F.; Markert, S.; Becher, D.; Fernandez-Guerra, A.; Liebeke, M.; Schweder, T.; Polz, M.F.; et al. Verrucomicrobia Use Hundreds of Enzymes to Digest the Algal Polysaccharide Fucoidan. *Nat. Microbiol.* **2020**, *5*, 1026–1039. [CrossRef]
9. Cundell, A.M.; Sleeter, T.D.; Mitchell, R. Microbial Populations Associated with the Surface of the Brown AlgaAscophyllum Nodosum. *Microb. Ecol.* **1977**, *4*, 81–91. [CrossRef]
10. Martin, M.; Barbeyron, T.; Martin, R.; Portetelle, D.; Michel, G.; Vandenbol, M. The Cultivable Surface Microbiota of the Brown Alga Ascophyllum Nodosum Is Enriched in Macroalgal-Polysaccharide-Degrading Bacteria. *Front. Microbiol.* **2015**, *6*, 1487. [CrossRef]
11. Cheng, W.; Yan, X.; Xiao, J.; Chen, Y.; Chen, M.; Jin, J.; Bai, Y.; Wang, Q.; Liao, Z.; Chen, Q. Isolation, Identification, and Whole Genome Sequence Analysis of the Alginate-Degrading Bacterium Cobetia Sp. Cqz5-12. *Sci. Rep.* **2020**, *10*, 10920. [CrossRef] [PubMed]
12. Reisky, L.; Préchoux, A.; Zühlke, M.-K.; Bäumgen, M.; Robb, C.S.; Gerlach, N.; Roret, T.; Stanetty, C.; Larocque, R.; Michel, G.; et al. A Marine Bacterial Enzymatic Cascade Degrades the Algal Polysaccharide Ulvan. *Nat. Chem. Biol.* **2019**, *15*, 803–812. [CrossRef] [PubMed]
13. Sun, Z.-Z.; Ji, B.-W.; Zheng, N.; Wang, M.; Cao, Y.; Wan, L.; Li, Y.-S.; Rong, J.-C.; He, H.-L.; Chen, X.-L.; et al. Phylogenetic Distribution of Polysaccharide-Degrading Enzymes in Marine Bacteria. *Front. Microbiol.* **2021**, *12*, 658620. [CrossRef] [PubMed]
14. Drula, E.; Garron, M.-L.; Dogan, S.; Lombard, V.; Henrissat, B.; Terrapon, N. The Carbohydrate-Active Enzyme Database: Functions and Literature. *Nucleic Acids Res.* **2022**, *50*, D571–D577. [CrossRef]

15. Hehemann, J.-H.; Boraston, A.B.; Czjzek, M. A Sweet New Wave: Structures and Mechanisms of Enzymes That Digest Polysaccharides from Marine Algae. *Curr. Opin. Struct. Biol.* **2014**, *28*, 77–86. [CrossRef]
16. Wang, S.; Lin, L.; Shi, Y.; Qian, W.; Li, N.; Yan, X.; Zou, H.; Wu, M. First Draft Genome Assembly of the Seaweed Sargassum Fusiforme. *Front. Genet.* **2020**, *11*, 590065. [CrossRef]
17. Zhang, R.; Zhang, X.; Tang, Y.; Mao, J. Composition, Isolation, Purification and Biological Activities of Sargassum Fusiforme Polysaccharides: A Review. *Carbohydr. Polym.* **2020**, *228*, 115381. [CrossRef]
18. Shao, Z.; Zhang, P.; Lu, C.; Li, S.; Chen, Z.; Wang, X.; Duan, D. Transcriptome Sequencing of Saccharina Japonica Sporophytes during Whole Developmental Periods Reveals Regulatory Networks Underlying Alginate and Mannitol Biosynthesis. *BMC Genom.* **2019**, *20*, 975. [CrossRef]
19. DeWeese, K.J.; Osborne, M.G. Understanding the Metabolome and Metagenome as Extended Phenotypes: The next Frontier in Macroalgae Domestication and Improvement. *J. World Aquac. Soc.* **2021**, *52*, 1009–1030. [CrossRef]
20. Lee, H.S.; Kwon, K.K.; Kang, S.G.; Cha, S.-S.; Kim, S.-J.; Lee, J.-H. Approaches for Novel Enzyme Discovery from Marine Environments. *Curr. Opin. Biotechnol.* **2010**, *21*, 353–357. [CrossRef]
21. Bolger, A.M.; Lohse, M.; Usadel, B. Trimmomatic: A Flexible Trimmer for Illumina Sequence Data. *Bioinformatics* **2014**, *30*, 2114–2120. [CrossRef]
22. Langmead, B.; Salzberg, S.L. Fast Gapped-Read Alignment with Bowtie 2. *Nat. Methods* **2012**, *9*, 357–359. [CrossRef]
23. Li, D.; Liu, C.-M.; Luo, R.; Sadakane, K.; Lam, T.-W. MEGAHIT: An Ultra-Fast Single-Node Solution for Large and Complex Metagenomics Assembly via Succinct de Bruijn Graph. *Bioinformatics* **2015**, *31*, 1674–1676. [CrossRef]
24. Gurevich, A.; Saveliev, V.; Vyahhi, N.; Tesler, G. QUAST: Quality Assessment Tool for Genome Assemblies. *Bioinformatics* **2013**, *29*, 1072–1075. [CrossRef]
25. Hyatt, D.; Chen, G.-L.; LoCascio, P.F.; Land, M.L.; Larimer, F.W.; Hauser, L.J. Prodigal: Prokaryotic Gene Recognition and Translation Initiation Site Identification. *BMC Bioinform.* **2010**, *11*, 119. [CrossRef]
26. Fu, L.; Niu, B.; Zhu, Z.; Wu, S.; Li, W. CD-HIT: Accelerated for Clustering the next-Generation Sequencing Data. *Bioinformatics* **2012**, *28*, 3150–3152. [CrossRef]
27. Qin, J.; Li, Y.; Cai, Z.; Li, S.; Zhu, J.; Zhang, F.; Liang, S.; Zhang, W.; Guan, Y.; Shen, D.; et al. A Metagenome-Wide Association Study of Gut Microbiota in Type 2 Diabetes. *Nature* **2012**, *490*, 55–60. [CrossRef]
28. Buchfink, B.; Xie, C.; Huson, D.H. Fast and Sensitive Protein Alignment Using DIAMOND. *Nat. Methods* **2015**, *12*, 59–60. [CrossRef]
29. Huson, D.H.; Auch, A.F.; Qi, J.; Schuster, S.C. MEGAN Analysis of Metagenomic Data. *Genome Res.* **2007**, *17*, 377–386. [CrossRef] [PubMed]
30. Bolyen, E.; Rideout, J.R.; Dillon, M.R.; Bokulich, N.A.; Abnet, C.C.; Al-Ghalith, G.A.; Alexander, H.; Alm, E.J.; Arumugam, M.; Asnicar, F.; et al. Reproducible, Interactive, Scalable and Extensible Microbiome Data Science Using QIIME 2. *Nat. Biotechnol.* **2019**, *37*, 852–857. [CrossRef]
31. Segata, N.; Izard, J.; Waldron, L.; Gevers, D.; Miropolsky, L.; Garrett, W.S.; Huttenhower, C. Metagenomic Biomarker Discovery and Explanation. *Genome Biol.* **2011**, *12*, R60. [CrossRef] [PubMed]
32. Cantalapiedra, C.P.; Hernández-Plaza, A.; Letunic, I.; Bork, P.; Huerta-Cepas, J. EggNOG-Mapper v2: Functional Annotation, Orthology Assignments, and Domain Prediction at the Metagenomic Scale. *Mol. Biol. Evol.* **2021**, *38*, 5825–5829. [CrossRef]
33. Alexa, A.; Rahnenfuhrer, J. TopGO: Enrichment Analysis for Gene Ontology. R Package version 2.48.0. 2022. Available online: https://bioconductor.org/packages/release/bioc/html/topGO.html (accessed on 21 July 2022).
34. Darzi, Y.; Letunic, I.; Bork, P.; Yamada, T. IPath3.0: Interactive Pathways Explorer V3. *Nucleic Acids Res.* **2018**, *46*, W510–W513. [CrossRef]
35. Huang, L.; Zhang, H.; Wu, P.; Entwistle, S.; Li, X.; Yohe, T.; Yi, H.; Yang, Z.; Yin, Y. DbCAN-Seq: A Database of Carbohydrate-Active Enzyme (CAZyme) Sequence and Annotation. *Nucleic Acids Res.* **2018**, *46*, D516–D521. [CrossRef]
36. Shannon, P.; Markiel, A.; Ozier, O.; Baliga, N.S.; Wang, J.T.; Ramage, D.; Amin, N.; Schwikowski, B.; Ideker, T. Cytoscape: A Software Environment for Integrated Models of Biomolecular Interaction Networks. *Genome Res.* **2003**, *13*, 2498–2504. [CrossRef] [PubMed]
37. Weigel, B.L.; Miranda, K.K.; Fogarty, E.C.; Watson, A.R.; Pfister, C.A. Functional Insights into the Kelp Microbiome from Metagenome-Assembled Genomes. *mSystems* **2022**, *7*, e01422–e01521. [CrossRef] [PubMed]
38. Lin, L.; Wang, F.; Wu, M.; Wang, S. DdRAD Sequencing-Based Scanning of Genetic Variants in Sargassum Fusiforme. *J. Mar. Sci. Eng.* **2022**, *10*, 958. [CrossRef]
39. Brunet, M.; de Bettignies, F.; Le Duff, N.; Tanguy, G.; Davoult, D.; Leblanc, C.; Gobet, A.; Thomas, F. Accumulation of Detached Kelp Biomass in a Subtidal Temperate Coastal Ecosystem Induces Succession of Epiphytic and Sediment Bacterial Communities. *Environ. Microbiol.* **2021**, *23*, 1638–1655. [CrossRef]
40. Zhang, Z.; Su, H.; Wang, X.; Tang, L.; Hu, J.; Yu, W.; Han, F. Cloning and Characterization of a Novel Chondroitinase ABC Categorized into a New Subfamily of Polysaccharide Lyase Family 8. *Int. J. Biol. Macromol.* **2020**, *164*, 3762–3770. [CrossRef]
41. Iwamoto, Y.; Araki, R.; Iriyama, K.; Oda, T.; Fukuda, H.; Hayashida, S.; Muramatsu, T. Purification and Characterization of Bifunctional Alginate Lyase from Alteromonas Sp. Strain No. 272 and Its Action on Saturated Oligomeric Substrates. *Biosci. Biotechnol. Biochem.* **2001**, *65*, 133–142. [CrossRef]

42. Hashimoto, W.; Miyake, O.; Ochiai, A.; Murata, K. Molecular Identification of Sphingomonas Sp. A1 Alginate Lyase (A1-IV') as a Member of Novel Polysaccharide Lyase Family 15 and Implications in Alginate Lyase Evolution. *J. Biosci. Bioeng.* **2005**, *99*, 48–54. [CrossRef]
43. Beleneva, I.A.; Zhukova, N.V. Bacterial Communities of Some Brown and Red Algae from Peter the Great Bay, the Sea of Japan. *Microbiology* **2006**, *75*, 348–357. [CrossRef]
44. Minich, J.J.; Morris, M.M.; Brown, M.; Doane, M.; Edwards, M.S.; Michael, T.P.; Dinsdale, E.A. Elevated Temperature Drives Kelp Microbiome Dysbiosis, While Elevated Carbon Dioxide Induces Water Microbiome Disruption. *PLoS ONE* **2018**, *13*, e0192772. [CrossRef]
45. Wietz, M.; Wemheuer, B.; Simon, H.; Giebel, H.-A.; Seibt, M.A.; Daniel, R.; Brinkhoff, T.; Simon, M. Bacterial Community Dynamics during Polysaccharide Degradation at Contrasting Sites in the Southern and Atlantic Oceans. *Environ. Microbiol.* **2015**, *17*, 3822–3831. [CrossRef] [PubMed]
46. Xu, F.; Chen, X.-L.; Sun, X.-H.; Dong, F.; Li, C.-Y.; Li, P.-Y.; Ding, H.; Chen, Y.; Zhang, Y.-Z.; Wang, P. Structural and Molecular Basis for the Substrate Positioning Mechanism of a New PL7 Subfamily Alginate Lyase from the Arctic. *J. Biol. Chem.* **2020**, *295*, 16380–16392. [CrossRef] [PubMed]